Architecture, electronic structure and stability of TM@Ge(n) (TM = Ti, Zr and Hf; N = 1–20) clusters: A density functional modeling

ARTICLE *in* JOURNAL OF MOLECULAR MODELING · MAY 2011

Impact Factor: 1.74 · DOI: 10.1007/s00894-011-1122-4 · Source: PubMed

3 AUTHORS, INCLUDING:

Debashis Bandyopadhyay
Birla Institute of Technology and Science Pi…

49 PUBLICATIONS **239** CITATIONS

SEE PROFILE

J Mol Model (2012) 18:405–418
DOI 10.1007/s00894-011-1122-4

ORIGINAL PAPER

Architecture, electronic structure and stability of TM@Ge(n) (TM = Ti, Zr and Hf; n = 1-20) clusters: a density functional modeling

Manish Kumar · Nilanjana Bhattacharyya · Debashis Bandyopadhyay

Received: 23 February 2011 / Accepted: 9 May 2011 / Published online: 28 May 2011

Abstract The present study reports the geometry, electronic structure and properties of neutral and anionic transition metal (TM = Ti, Zr and Hf)) doped germanium clusters containing 1 to 20 germanium atoms within the framework of linear combination of atomic orbitals density functional theory under spin polarized generalized gradient approximation. Different parameters, like, binding energy (BE), embedding energy (EE), energy gap between the highest occupied and lowest unoccupied molecular orbitals (HOMO-LUMO), ionization energy (IP), electron affinity (EA), chemical potential etc. of the energetically stable clusters (ground state cluster) in each size are calculated. From the variation of these parameters with the size of the clusters the most stable cluster within the range of calculation is identified. It is found that the clusters having 20 valence electrons turn out to be relatively more stable in both the neutral and the anionic series. The sharp drop in IP as the valence electron count increases from 20 to 21 in neutral cluster is in agreement with predictions of shell models. To study the vibrational nature of the clusters, IR and Raman spectrum of some selected TM@Ge_n (n= 15,16,17) clusters are also calculated and compared. In the end, relevance of calculated results to the design of Ge-based super-atoms is discussed.

Keywords Binding energy · Clusters and nanoclusters · Density functional theory · Electron affinity · Embedding energy · Ionization potential · IR and Raman

M. Kumar · N. Bhattacharyya · D. Bandyopadhyay (✉)
Physics Department, Birla Institute of Technology and Science, Pilani, Rajasthan 333031, India
e-mail: Debashis.bandy@gmail.com

D. Bandyopadhyay
e-mail: bandy@bits-pilani.ac.in

Introduction

In the last few decades study of electronic structures and properties of silicon and germanium based semiconductor nanoclusters has been an extremely active area of research due to its importance in nanoscience and nanotechnology [1–9]. Theoretical modeling of semiconductor nanoclusters with modified new geometries show possibility of using them as nano-devices in opto-electronics, tunable lasers, sensors, etc. The results of the theoretical modeling also show that it is possible to integrate wide area of photonics with electronics by designing miniature devices using pure and hybrid semiconductor nanoclusters [10, 11]. Therefore, modeling of pure and hybrid semiconductor nanoclusters is a very interesting and important field in theoretical and computational research with supporting experimental results. It is always challenging to produce experimentally or model theoretically the stable and nonreactive nanoclusters of different compositions of interest from the application point of view. It is known that pure semiconductor nanoclusters are chemically reactive, but encapsulation of transition metal atom/atoms by pure semiconductor clusters enhances the stability of the clusters and simultaneously exhibits much novel behavior. The increase in stability of the semiconductor clusters when doped with transition metal atom/atoms is due to the fact that the transition metal atom can absorb the dangling bonds present on the pure semiconductor cage or cluster surface [12–17]. An important experimental contribution on such nanoclusters was made by Beck [18, 19] by using laser vaporization supersonic expansion technique. It showed that addition of the transition metals like, Cr, Mo W etc. in silicon clusters enhanced the stability of the doped clusters compared to the same size pure silicon semiconductor clusters by subjecting them to photo-fragmentation. Hiura

et al. [7] reported the formation of a series of stable silicon cages with transition-metal atoms Hf, Ta, W, Re, Ir etc. O'hara et al. [20] studied the geometric and electronic structures of the negatively charged Tb doped silicon clusters with photoelectron spectroscopy and chemical-probe method, and proved that Tb atom always remains encapsulated inside the silicon clusters made of ten silicon atoms. Recently, Bandyopadhyay [15, 16] reported an extensive study of the electronic structure, growth behavior, different physical and chemical properties of the pure and transition metal doped silicon clusters ($TM@Si_n$, TM = Ti, Zr and Hf, n=9-20). It is found that the metal-doped fullerene like $Si_{16}TM$ (TM = Ti, Zr and Hf) clusters are chemically the most stable species in the whole series of study. Compare to silicon nanoclusters there is not much report on the investigation of germanium nanoclusters theoretically as well as experimentally. Some of the recent investigations on pure and halogen-doped germanium clusters are mainly focused on optimized geometries, binding energies, ionization potential, electron affinities etc. [2, 7, 18–21]. A few theoretical and experimental contributions have been made by different groups on the endohedral doping of transition metal (TM) elements in pure and hydrogenated Ge cages [22–25]. Even after several studies of pure and hybrid silicon and germanium nanoclusters, there is no clear scientific way to explain the cause of the stabilities of nanoclusters of a particular size in a system. From famous "electron counting rule" point of view it is not clear whether their relative stability obeys 18-electron counting rule (also known as the octet rule) or 20-electron counting rule [26]. Following 18-electron rule $Si_{12}Cr$ and $Si_{12}W$ should be the most stable clusters in the 3 d and 5 d TM doped Si_n series respectively. Recent investigations showed the electron counting rule sometimes a valid explanation for stability, but not always [27–29]. It is well known that the stability depends upon the nature of transition metal atoms. In addition, one needs to follow the free-electron gas theory and Wigner-Witmer (WW) spin conservation rule [30] while calculating embedding energies (EE) to explain the stability of the cluster. However, the free-electron gas picture is not valid in every case because it is found that the anionic $Si_{12}Mn$ and $Si_{12}Co$ show maximum value in embedding energy curve whereas they are 20 and 22-electron clusters respectively according to electron counting rule [29]. On the other hand, experiments have supported the validity of these electron-counting rules in some cases. Koyasu et al. [31] studied the electronic and geometrical structures of $Si_{16}TM$ (TM = Sc, Ti, and V) clusters using mass spectrometry and anion photoelectron spectroscopy. They found that neutral $Si_{16}Ti$, being a 20-electron cluster, had a closed-shell electron configuration with a large HOMO-LUMO gap. Recently Bandyopadhyay [15, 16] also found similar behavior in density functional studies of $TM@Si_n$ (TM = Ti, Zr and Hf) system.

With this background work, the present study makes an effort to explain the enhanced stability of $TM@Ge_{16}$ (TM = Ti, Zr and Hf) clusters by calculating different parameters of the ground state cluster in each size within the size range of 1 to 20 germanium atoms using density functional theory (DFT). Although Ti-doped Ge_n clusters have been theoretically studied before [32], this study was limited to a particular size range. The main focus of the present study is to explain the relative stability of these clusters in neutral and cationic state in the range from n =1-20 in view of electron counting rules and also to study their chemical and vibrational properties.

Computational methods

In the present report the theoretical calculations are performed within the framework of linear combination of atomic orbitals density functional theory under spin polarized generalized gradient approximation. The exchange-correlation potential contributions are incorporated in the calculation by using generalized gradient functional (GGA) proposed by Perdew-Wang (B3PW91) [33–36]. Molecular orbitals are expressed as linear combination of atom-centered basis functions for which the standard Gaussian basis (LanL2DZ) associated with effective core potential (ECP) is used on all atoms. This basis set can reduce the difficulties in two-electron integrals caused by the transition metal atoms [37–40]. All geometry optimization calculations are performed under no external symmetry constrictions. It is always possible that during optimization the cluster can get trapped in local minima of the potential energy surface. To avoid it during optimization in a particular size, several geometrical initial guess configuration at different spin states (sometimes varied from singlet to septet) were used to search for the ground state and higher energy isomers. In case when total optimization energy decreases with increasing spin, increasing higher spin states is considered until energy minima with respect to spin is reached. For small clusters, considered in this work, such an approach provides a fairly extensive search of the potential energy minima. In order to check the validity of the applied methodologies, a trial calculation is carried out on Ge-Ge dimer. Calculated Ge-Ge bond length is 2.54 Å which is within the range of the values obtained theoretically as well as experimentally reported by Nagendran et al. [41]. The optimized electronic structure was obtained by solving the Kohn–Sham equations self-consistently [42] where default optimization criteria of Gausssian-03 [43] are followed. Initial geometries of the clusters are constructed on the basis of the reported structures [2, 3] and from

intuitions. Equilibrium structure in a particular size is obtained by varying the geometry starting from high to low symmetric initial guess structures. For each stationary point of a cluster, the reliability of the clusters is reassured by calculating the frequency of harmonic vibration (IR and Raman). If any imaginary frequency is found, a relaxation along that vibrational mode is carried out until the true local minimum is obtained. Broadening is applied on the calculated frequencies to plot the IR and Raman response of the clusters, which is a default criterion of Gauss View 03 program package. In each size, identical sets of initial geometries are used for Ti, Zr and Hf doped germanium clusters to see their growth behavior. Geometry optimizations were carried out with a convergence limit of 10^{-7} Hartree on the total electronic energy. The optimized electronic structure for each cluster is obtained from the *Z*-matrices in the program output, where as electronic properties were calculated from the SCF total electronic energy and the orbital energy values. All theoretical calculations are performed with GAUSSIAN-03 program package [43].

Results and discussion

In our previous report [11] a detailed study of the growth behavior of pure germanium cluster is presented. Therefore, in the report the growth behavior of different transition metal (Ti, Zr and Hf) doped germanium clusters will be discussed.

Growth of hybrid Ge_nTM nanoclusters

Since the growth evolution pattern of Ti, Zr and Hf are similar, therefore, in the following section the growth behavior of $Ti@Ge_n$ will be presented with related discussion of Zr and Hf doped germanium clusters. Calculated optimized geometries within the size range of n=1-20 are shown in Fig. 1 with the relative energy of the ground state $Ti@Ge_n$ clusters in each size. In the same figure the ground state geometries of Zr and Hf doped clusters for n=9-20 size range are also presented. A number of isomers are calculated in each size. But only selected isomers those are close to the ground state structures are presented in Fig. 1. The present report is mainly based on the Ti doped germanium cluster and hence it is necessary to mention the basic properties of titanium. It is well known that titanium is paramagnetic material with $Ar3d^24s^2$ electronic configuration and electro-negativity 1.91 in Pauling scale. When germanium cluster doped with titanium, in most of the case sp^3d^2 hybridization with the germanium atoms in the clusters takes place.

The first structure of Ge_nTM (TM = Ti, Zr and Hf) series is a dimer optimized for singlet, triplet, quintet and septet spin states. It is found that Ge-Ti dimer in quintet spin state is the optimized ground state (GS). The next ground state optimized structure for n=2 is in triplet spin state for all TM doped clusters. At this size, only four possible geometries can be constructed and all four different structures are optimized. Among these four, the triangular structure $Ge_2(A)TM$ is the optimized ground state structure. The second structure is a bent structure (Ge-TM-Ge) with an internal angle 44.67^0 for $Ti@Ge_2$. Other two structures are linear chain structures with the metal atoms are positioned at the end (Ge-Ge-TM) or at the middle of the chain (Ge-TM-Ge). In Ge_3TM, three different optimized geometries (two rhombi and a pyramid) are optimized. In the planer rhombi structures position of TM metal atoms are different as shown in Fig. 1. The rhombus like structure $Ge_3(A)TM$, in triplet spins is found as ground state.

In Ge_4TM family, five different isomers are optimized with a $Ge_4(A)TM$ in triplet spin state as GS structure (Fig. 1). This structure can be obtained by capping a TM atom on a Ge_4 (bent rhombus) structure. Other optimized isomers are mainly planar structures with transition metal atom positioned at different sites. These structures are 'planar pentagon' and 'rhombus with a tail' like structures in different forms as shown in Fig. 1. Three different structures are obtained in Ge_5TM size (Fig. 1) with small difference in their optimized energy. The ground state structure in triplet spin state looks like a bi-capped quadrilateral where one capped atom is Ge and the other one is TM. Change in position of TM atom in the cluster can give other isomers as shown in Fig. 1. Three different optimized geometries in Ge_6TM series are shown in Fig. 1. These structures are based on the ground state structure of $Ge_6(A)$ and $Ge_7(A)$ as reported by Bandyopadhyay and Sen [11]. The optimized triplet ground state structure $Ge_6(A)$ TM is obtained by adding one TM atom on the side triangular plane of $Ge_6(A)$ ground state structure or by replacing the capped germanium atom by TM and adding one extra germanium atom on the bi-capped pyramidal plane of $Ge_6(A)$ structure. Other structures shown in Fig. 1 can be obtained by replacing one germanium atom in $Ge_7(A)$ cluster [11] from different positions. Addition of one TM atom with one of the side planes of $Ge_7(A)$ pure structure gives optimized ground state structure in triplet spin state $Ge_7(B)TM$ as shown in Fig. 1. With increasing the number of germanium atoms in the cluster, the tendency to encapsulate TM atom in stable structures increase. In the ground state $Ge_8(C)Ti$ structure, the Ti atom is outside the germanium cluster. It is possible to optimized a structure with endohedrally capped TM although it is not the GS structure in this size. Following the reported geometries available in literatures [2, 3] and also some more new geometry constructed from intuition, with an aim to encap-

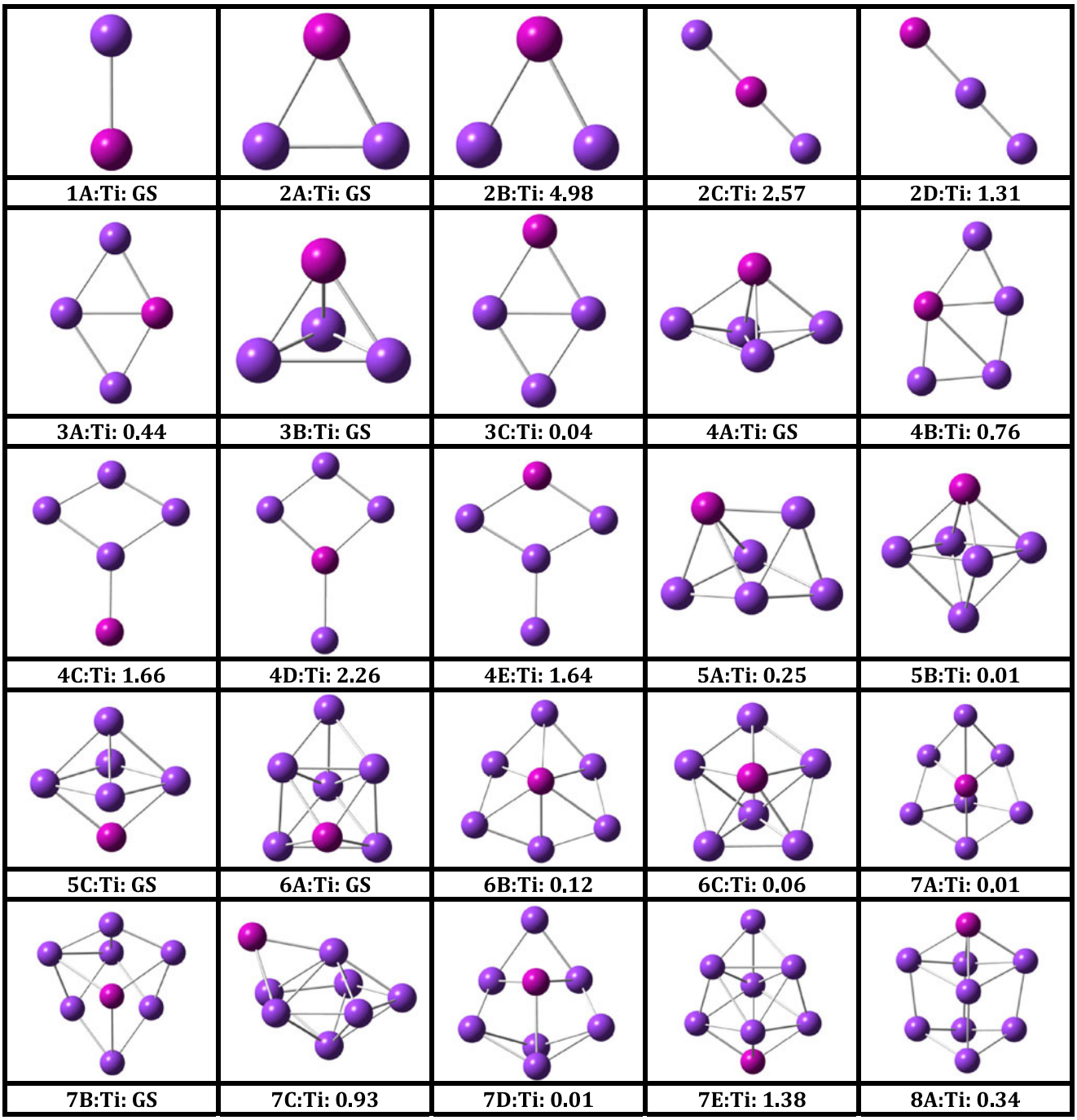

Fig. 1 Optimized structures of pure Ge_nTi and some selected Ge_nZr and Ge_nHf clusters for n=1 to 20. The dip purple colored solid spheres in the clusters represent Ge atoms. The numeric given next to the cluster name represents the relative energies of the optimized geometries in eV with respect to the ground state cluster of same size

sulate the titanium atom endohedrally, three different geometries are taken as initial guess structures to search for the optimized ground state in TM@Ge_n series. The structures Ge_9(A)TM and Ge_9(C)TM as shown in Fig. 1 absorb transition metal atom endohedrally in optimized state. The third structure Ge_9(B)TM is the ground state and it absorbs the transition metal atom exohedrally on the Ge_9 surface. The optimized ground state isomer Ge_9(B)Zr and Ge(B)Hf also absorb the TM atoms exohedrally on the Ge_9 cluster surface. Therefore up to this size the endohedrally doped structures are energetically not favorable.

In the next series, $Ge_{10}Ti$, a number of optimized structures are found; out of those structures only four different structures have been reported here. The first

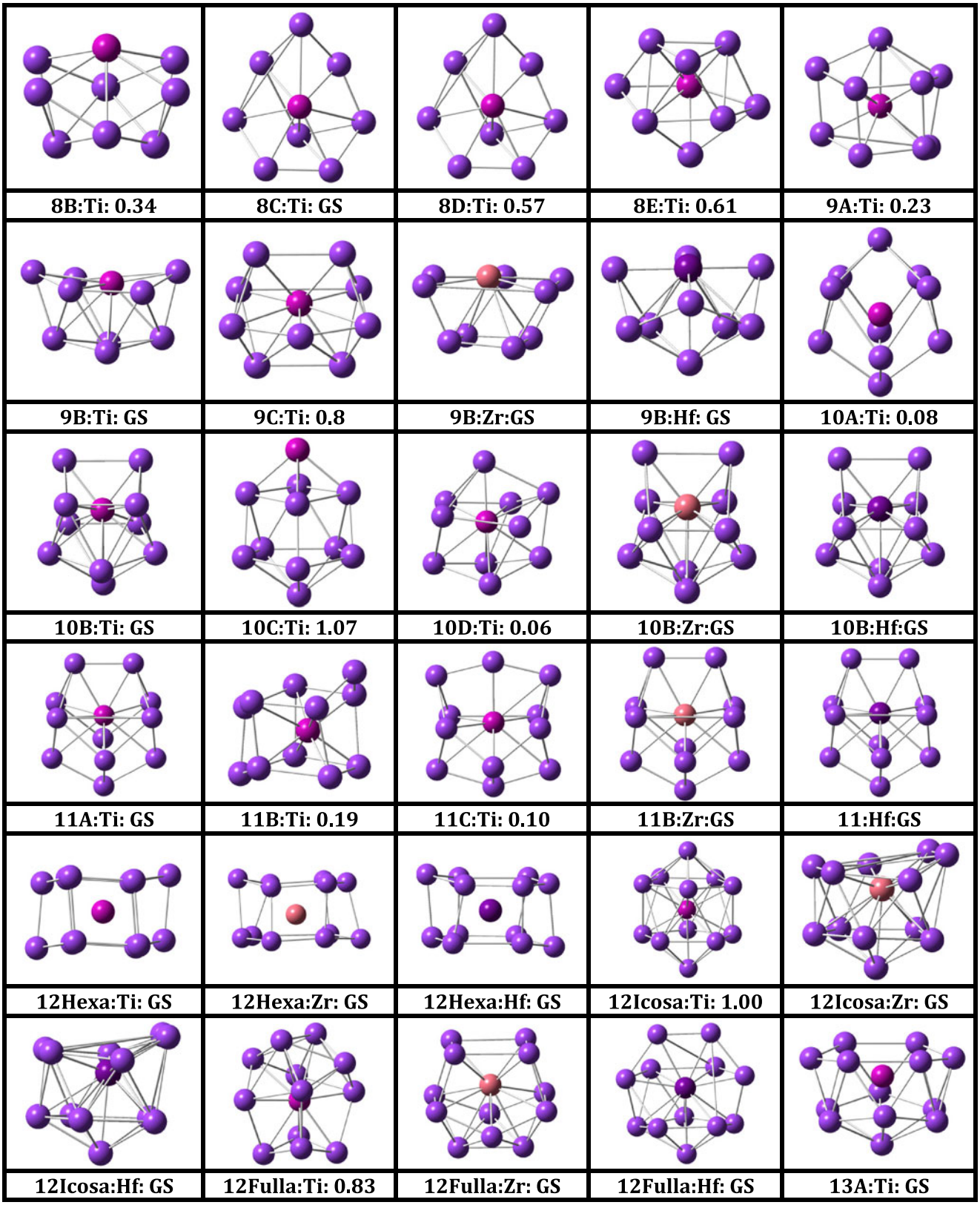

Fig. 1 (continued)

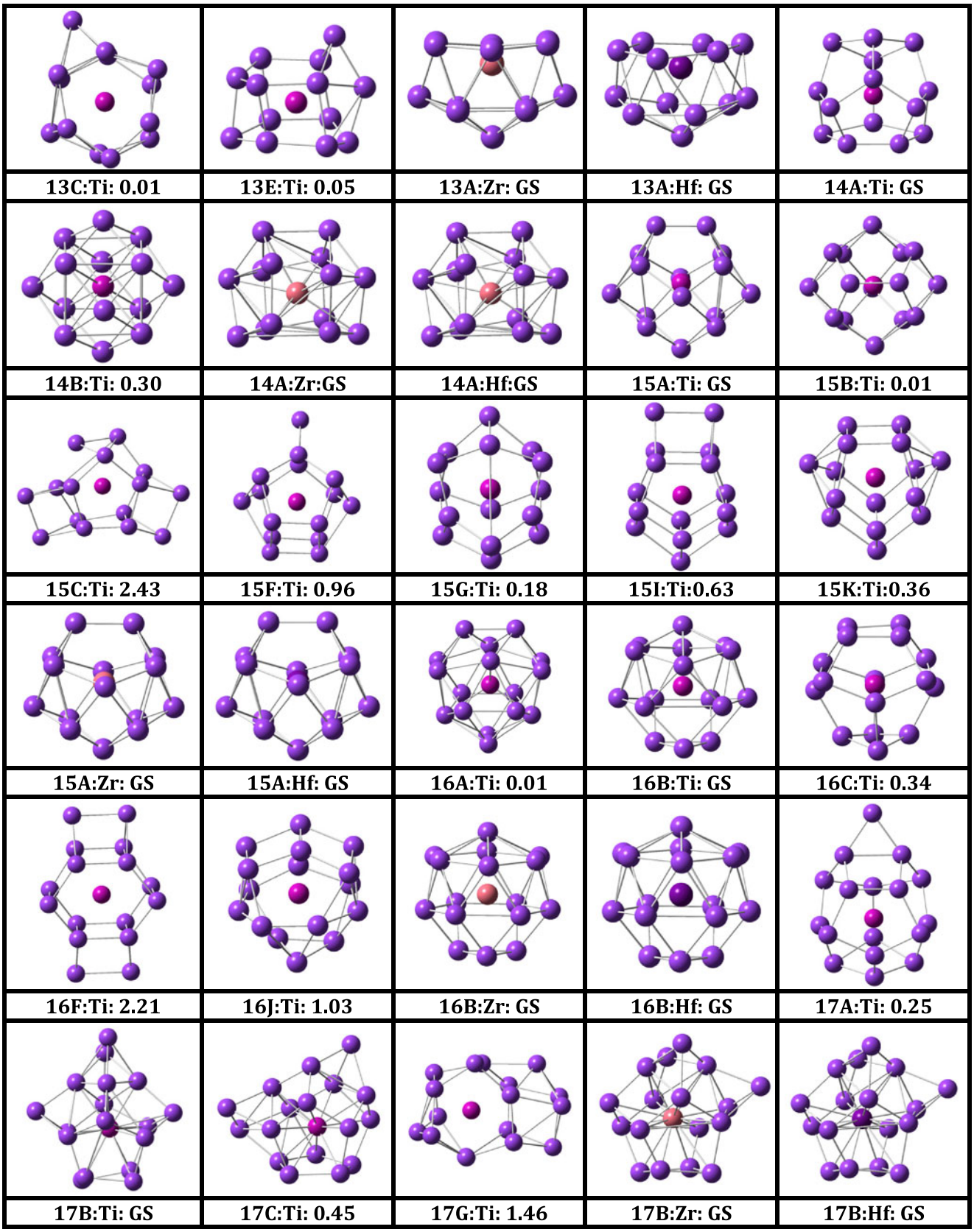

Fig. 1 (continued)

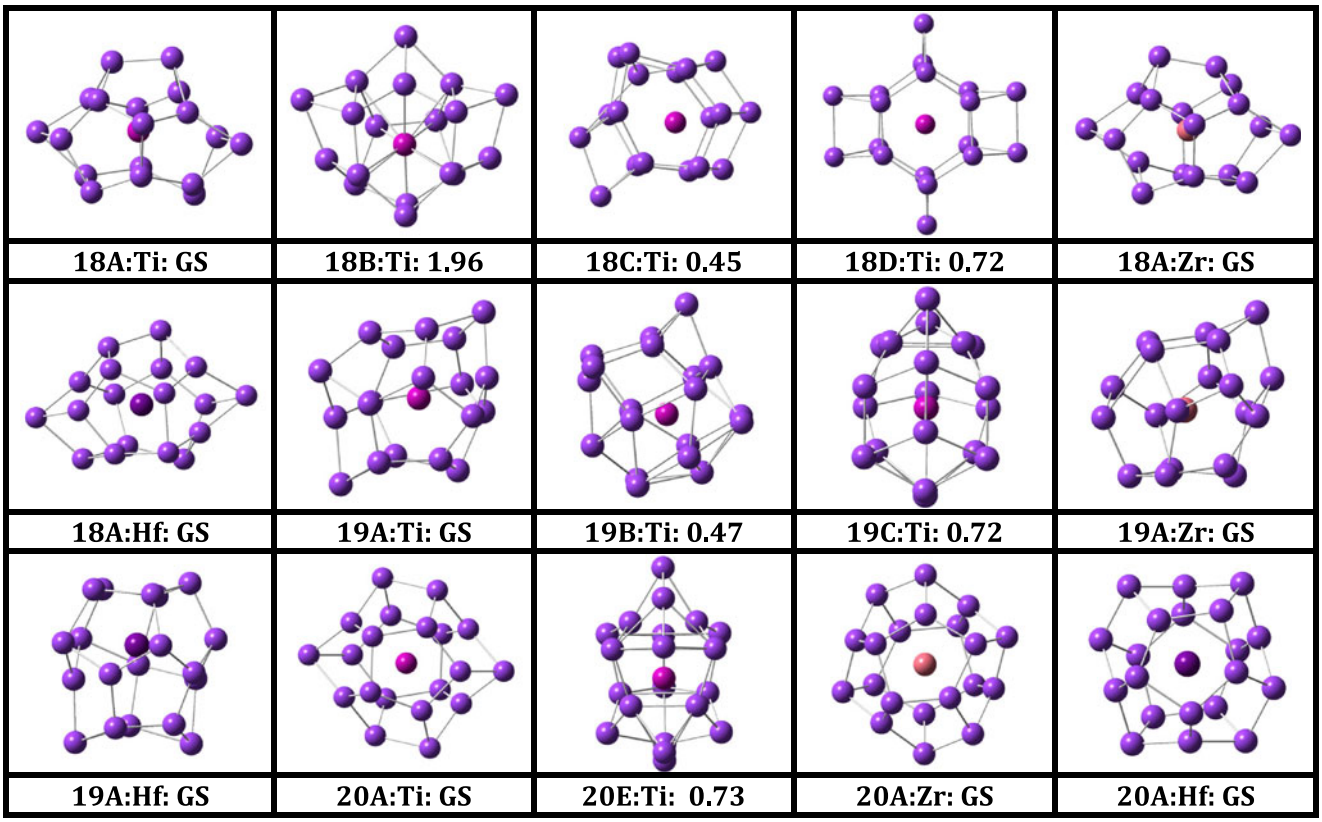

Fig. 1 (continued)

optimized structure Ge_{10}(A)Ti is a combination of pentagonal and rhombus planes capped by the germanium atom. The second structure Ge_{10}(B)Ti, is the first in this series that can give GS geometry by absorbing Ti atom endohedrally as shown in Fig. 1. The third and the fourth structures absorb Ti atom exohedrally and endohedrally respectively. For n=11 we obtained three endohedrally absorbed TM doped structures. The structure Ge_{11}(A)TM is the ground state for all Ti, Zr and Hf as shown in Fig. 1. Out of five optimized geometries, three important optimized geometries, known as hexagonal, fullerene and icosahedral structures in Ge_{12}TM series are presented in Fig. 1. Among these three structures in different spin states, the relaxed hexagonal singlet spin state structure is the ground state. In some transition metal doped Ge_{12} fullerene-like structures (combination of four pentagons and four rhombi) show ground state. It is known that this kind of pentagon and rhombi combination always gives better stability [14]. In this context it is important to mention that transition metal-doped fullerene-like structure is not always the ground state isomer. It depends upon the nature of transition metal doping [39]. As example the Cu doped fullerene structure is not a ground state structure for n =12 size. According to previous investigations on the transition metal (Ti, Zr and Hf) encapsulated silicon clusters, the metal-encapsulated hexagonal prism is proven to be the lowest-energy structure [15, 16]. In another study the optimized Ge_{12}Zn icosahedral isomer is lower in energy than the hexagonal prism structure [44, 45]. Therefore, it is clear that in n=12 size, the ground state structure is strongly depends on the transition metal doping. Careful observation show that the ground state structures from Ge_9(A)Ti to Ge_{11}(A)Ti are all of similar kinds and follow a common trend in their growth behavior. Several initial guess geometries are optimized in Ge_{13}TM series. Out of them three optimized structures including the ground state Ge_{13}(A)TM geometry are presented in Fig. 1. The other geometries are very similar in structure to the GS state geometry with a minor difference in energy. Therefore in the present report those geometries are not presented. The ground state Ge_{13}(A)TM structure is hexagonal capped bowl kind of structure with transition metal atom inside. It is to be noted that the binding energy presented in Fig. 2 show clear two trend of variation of binding energy with the size of the cluster for pure and doped clusters. For n<8, the binding energy of the pure clusters are more than the doped clusters of same size, whereas, for n>8, the trend is reversed. This is because of the absorption of the dangling bonds of the germanium cage by the endohedrally doped TM atom [46]. By adding one germanium atom with Ge_{13}(A)TM one can form the optimized ground state structure Ge_{14}(A)TM with threefold symmetry in Ge_{14}TM series. Out of the other three optimized geometries, Ge_{14}(A)TM is presented in Fig. 1.

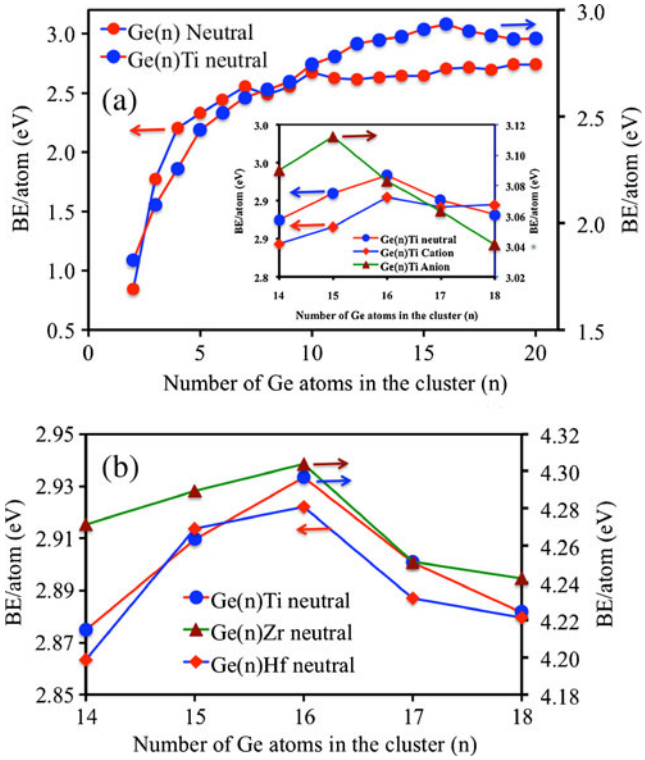

Fig. 2 Variation of binding energy of Ge_nTM with the size of the cluster (n)

The ground state structure Ge_{14}(A)TM has threefold symmetry. It contains six pentagons and three isolated rhombi. Again this structure confirms that the structures with pentagons and isolated rhombi are more favorable and follow the isolated rhombus rule [46] in carbon fullerene. The second optimized isomer Ge_{14}(B)TM is a symmetrical hexagonal bi-capped structure with total eight rhombi. The optimized ground state structure of Ge_{15}(A)TM is quite similar to Ge_{14}(A)TM. It is easy to understand the Ge_{15}(A) TM initial guess structure by adding one germanium atom to the bottom of the rhombi in Ge_{14}(B)Ti and then replace Ti by the transition metal atom. The optimized Ge_{15}(A)TM structure consists of two connected pentagons and ten rhombi. At this size a total of 11 guess structures are optimized. Out of these 11 structures, only the cage like structures, those which are close to the energy of the ground state structures are presented in Fig. 1. In the next size Ge_{16}TM, ten initial guess geometries are optimized and five are presented. With the increase of the size of the clusters, possibility of searching the ground state structure is always a difficult job. Therefore the numbers of initial guess geometry also increase so that the ground state structures can be obtained. Out of the ten optimized geometries, cage kind five structures are presented in Fig. 1. The geometry of the ground state Ge_{16}(B)TM structure can be understand on the basis of the ground state structure of Ge_{12}TM by capping the hexagonal planes using one Ge and a Ge_3 planer triangle structure. When the hexagonal planes in Ge_{12}Ti structure is capped by two crossed Ge-Ge dimers, optimized Ge_{16}(A)Ti structure is obtained. The other structure Ge_{16}(C)Ti has two widely separated squares and eight pentagons. Each square is connected to four pentagons separately. This structure is not as symmetrical as found in titanium doped silicon cluster of same size [15, 16]. It is to be noted that with the increase of the size of the clusters beyond n=16, distortion starts in the structures and it continues up to the biggest structure for n= 20 in most of the geometries. In this contest it is worth mentioning that the pure and transition metal doped all Ge_nH_n (n=6-28) clusters are very symmetrical [25] because of the strong bonding between the hydrogen and the germanium atoms in the cluster surface. The hydrogen atoms absorb the unsaturated dangling bonds in the cage and give a symmetrical structure. Other bigger clusters in the present study also show distorted structures. Optimized Zr and Hf doped ground state germanium clusters for n>13 are presented in Fig. 1. These structures are similar to the Ti doped germanium clusters of same size. In summary, the growth behavior of TM@Ge_n (TM = Ti, Zr and Hf) doped germanium clusters follow two different trends. In lower range of the cluster size (n<10), the geometry of the cluster changes from planner to three-dimensional ground state structure where the TM atom absorbs either exohedrally or stays as surface capped element with the germanium clusters. From n=1-7, TM elements attached with the germanium clusters as an exohedrally connected element. For n=8, the TM atom absorbs partially in optimized ground state cluster Ge_8(A)TM. In the next stage of growth of the clusters, TM atoms absorb endohedrally in GS state geometry for n=9 and then form a cage like cluster for n>9 as ground state geometry. The cages are very much symmetric up to n=16 and for bigger clusters, the TM atoms stay inside the cage cluster, but the cage gets distorted in some isomers. Depending on the cage size and combination of pentagons, rhombi and hexagons, sometimes in bigger sizes (i.e., n=24), it is also possible to get a symmetrical optimized TM doped cage like germanium clusters as ground state [2].

In the next section different physical and chemical properties of the neutral as well as the charged clusters will be discussed.

Electronic structure and stabilities of TM@Ge_n nanoclusters

In the present section the electronic structure and stabilities of the TM@Ge_n (TM = Ti, Zr and Hf) clusters of different size will be discussed by calculating their binding energy (BE), HOMO-LUMO gap (or ΔE), embedding energy (EE), relative stability (Δ_2), ionization potential (IP) etc. Following the behavior of these parameters with the cluster size, we will investigate whether the electron-counting rule can explain the relative stability of the clusters or not.

To explore the relative stability of Ge_nTM clusters with the increasing number of 'n' from n=1 to 20, binding energy (BE), embedding energy (EE), HOMO-LUMO gap (ΔE), and the relative stability or second order energy difference (Δ_2) of the clusters are studied.

In the present calculation, binding energy per atom following WW rule [30] of the clusters is defined as follows:

$$BE = -(E_{Ge_nTM} - nE_{Ge} - E_{TM})/(n+1), \quad (1)$$

where BE is the binding energy per atom in the cluster $TM@Ge_n$, E_{GenTM}, E_{Ge} and E_{TM} are the ground state energies of $TM@Ge_n$ cluster, germanium and transition metal atoms respectively. Following the same expression, binding energy of the anion clusters is also calculated. The variation of binding energy of different clusters both in neutral and charged states are shown in Fig. 2a–b. In Fig. 2a the graphs show the rapid increase in binding energy per atom of the clusters in small size range from n=1 to 9 indicating thermodynamic instability of the small size clusters. For the sizes n>9 the binding energy curve increase with relatively lower rate. It is to be noted that for n=16 and n=15 in neutral and anion clusters, binding energy show maximum values in the whole range of study. Both of these clusters are 20-electron cluster. Signature of 20-electron cluster in cationic state is not very clear in the binding energy variation. The relative change in BE per atom in cationic cluster for n=15-17 is in the range of ±0.01 eV or even less. Therefore it is not presented in the variation of other parameters with the size of the cluster. There is no significant change in binding energy in the graphs for n=14 (or 13 in anion) and n=18 (or 17 in anion) sizes so that these clusters cannot be justified as 18 or 22 electron clusters. Presence of relative peak in the binding energy graphs for n=12 could be due to the higher relative stability of the geometry of the cluster. Variation of BE of the other transition metal clusters is shown in Fig. 2b. The nature show that Zr and Hf doped clusters are also show maximum values in binding energy for n=16. The next parameter that can indicate the thermodynamic stability of the cluster is embedding energy (EE). In the present study embedding energy of the cluster is defined as:

$$EE = -(E_{Ge_n} + E_{TM} - E_{Ge_nTM}) \quad (2)$$

which, is always negative. As before, E_{Ge_nTM} and E_{Ge_n} are the ground state energy of Ge_nTM and Ge_n clusters, E_{TM} is the energy of the TM atom. The above equation can be modify by imposing WW spin conservation rule [30] as follows:

$$EE^{WW} = {}^{M}E_{Ge_nTM} - {}^{M}E_{Ge_n} - {}^{0}E_{TM} \quad (3)$$

where M is the total spin of the cluster or of the atom in unit of $\hbar/2$. For example if the cluster is in triplet state, in calculating the embedding energy we have to take either the energy of the TM atom in triplet state with pure germanium cluster in singlet spin state or the pure germanium cluster in triplet spin state with singlet titanium atom. More precisely, in such case one has to take the value where EE is relatively less. Therefore, in our present calculation, for smaller size clusters where the spin states are not singlet, the EE is calculated according to the above method. It is necessary to mention that, taking the energy of TM atom in triplet state in a series of EE calculation does not make any relative change, because it will shift the graph by an amount of energy $E^3_{TM} - E^1_{TM}$. So the nature of the graph will remain unchanged. Therefore, whether it is necessary to include WW rule [30] in calculating the relative stability always or to follow different method for different transition metal doped germanium clusters is not possible to say. In the present calculation since there is only one TM atoms from the 2nd column of the periodic table, so WW rule [30] in calculating relative stability is included. For the charged clusters the situation gets a little more complicated. In case of $Ti@Ge_n$ clusters the excess charge can be either on the Ge_n cluster or on the Ti atom. Hence we have to consider both of these possibilities, and take whichever is smaller. In such case EE for anionic can be written as:

$$EE\left({}^{M}Ge_nTi^{-}\right) = {}^{M}E_{Ge_nTi^{-}} - {}^{1}E_{Ge_n^{-}} - {}^{M\pm1}E_{Ti} \; or \; {}^{M}E_{Ge_nTi^{-}} - {}^{0}E_{Ge_n^{-}} - {}^{M}E_{Ti} \quad (4)$$

Variation of EE with size (n) for both neutral $TM@Ge_n$ and anionic $Ti@Ge_n$ clusters are shown in Fig. 3. In the neutral clusters, EE is minimum at n=16. Interestingly, in the anionic clusters, EE has a dip at n=15. Thus both in the neutral and cationic series, 20-electron clusters have enhanced stability. The dip in EE graph indicates the most favorable size (here n=16) and geometry of pure germanium cluster to incorporate a TM atom. To further check the most stable cluster in the Ge_nTM series during its growth from n=1 to n=20, Ge atom is added one by one to Ge-TM dimer and the stability parameter is calculated. The stability

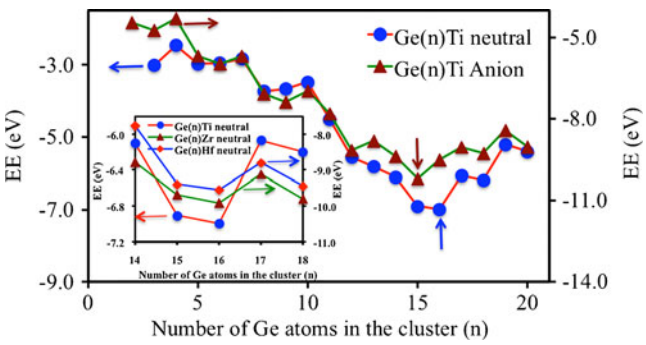

Fig. 3 Variation of embedding energy of Ge_nTM with the size of the cluster (n). In the figure vertical arrows represent the position of 20-electron cluster in the graph

parameter $\Delta_2(n)$ is defined by following previously reported work [11] as follows:

$$\Delta_2(n) = \left(E_{Ge_{n+1}TM} - E_{Ge_nTM}\right) - \left(E_{Ge_nTM} - E_{Ge_{n-1}TM}\right) \quad (5)$$
$$= E_{Ge_{n+1}TM} + E_{Ge_{n-1}TM} - 2E_{Ge_nTM}$$

According to this definition, large positive values of $\Delta_2(n)$ are indicative of enhanced stability as they correspond to a gain in energy during formation from the preceding size and lower gain in energy to the next size. Variation of stability with the size of the neutral and anionic clusters is shown in Fig. 4. Presence of peak position at n=16 and n=15 for neutral and anionic clusters respectively are representing the enhanced stability of these clusters. Both of these clusters are again supporting the enhanced stability in 20-electron clusters like binding energy and embedding energy graphs discussed before. In general the clusters which are in magic (positive stability) in neutral states remain magic in most of the negatively charged state.

To see the nature of the growth behavior around n=16 cluster which is a 20-electron cluster, fragmentation energy, Δ(n,n-1) or FE of the clusters in each step starting from Ge-TM dimers is calculated. Here fragmentation energy is defined as follows:

$$\Delta(n, n-1) = -\left(E_{Ge_nTM} - \left(E_{Ge_{n-1}TM} + E_{Ge}\right)\right) \quad (6)$$
$$= E_{Ge_{n-1}TM} + E_{Ge} - E_{Ge_nTM}$$

Figure 5 represents the variation of FE with the cluster size. It is clear that there is a sharp drop in FE form n=16 to 17 in neutral state and from n=15 to 16 in anionic $Ge_{16}Ti$ cluster. This is an indication of the sudden change in stability from n=16 (or n=15) to n=17 (or n=16) in neutral (or anionic) state. Behavior of fragmentation energy variation of Zr and Hf doped germanium clusters within the size range 14≤n≤18 is also shown in Fig. 5. In all doped clusters FE drop sharply when it changes from n=16

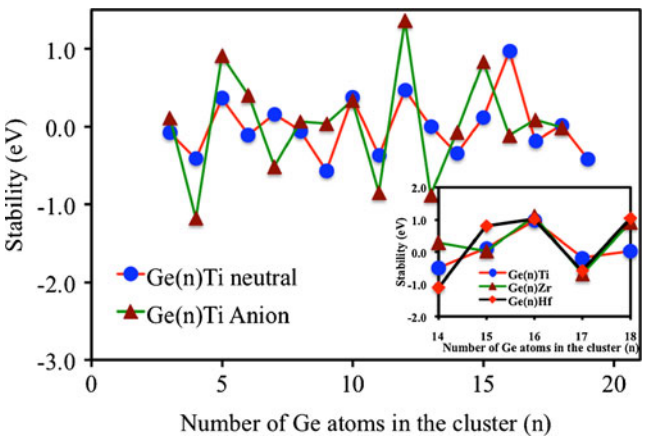

Fig. 4 Variation of stability of Ge_nTM with the size of the cluster (n)

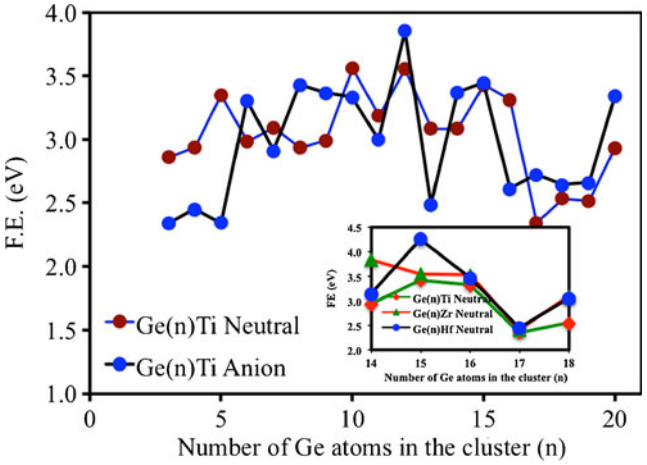

Fig. 5 Variation of fragmentation energy of Ge_nTM with the size of the cluster (n)

to 17. This is an indication of higher stability of the clusters at n=16 size. Therefore, it is clear that BE, EE and $\Delta_2(n)$ support the relatively higher thermodynamic stability of the clusters for n =16 and 15 in neutral and anionic states respectively.

To get the idea about the kinetic stability of the clusters in chemical reactions the HOMO-LUMO gap (ΔE), ionization potential (IP), electron affinity (EA), chemical potential (μ), chemical hardness (η) and their ratio (−μ/η|) are calculated. In general with the increase of HOMO-LUMO gap the reactivity of the cluster decrease. HOMO-LUMO gaps of neutral and anionic GenTM clusters are plotted in Fig. 6. Overall, there is a decrease of the HOMO-LUMO gap with the size of the clusters both in neutral and anionic state with some local oscillations over and above the decreasing trend. It is to be noted that these clusters have large HOMO-LUMO gap varies between 1.00 to 3.13 eV. Although there is no sharp global peak as in other parameters as discussed, there is a clear local peak at n=16

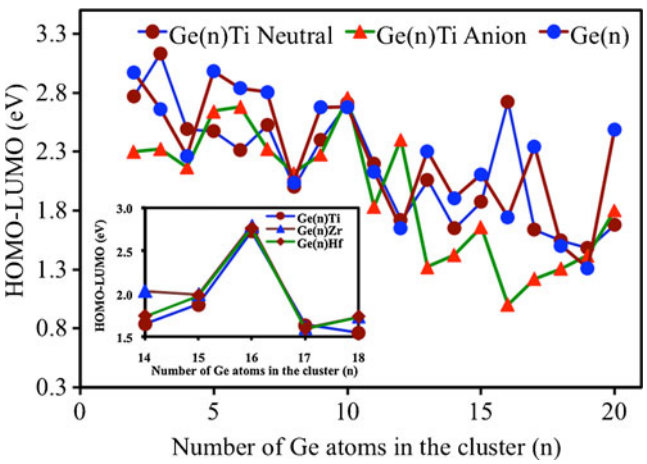

Fig. 6 Variation of HOMO-LUMO gap of Ge_nTM with the size of the cluster (n)

and 15 in neutral and anionic Ge_nTi clusters. This again points to an enhanced stability of 20-electron clusters. It is also worth noticing that at almost all sizes there is a decrease in the HOMO-LUMO gap on TM (Ti, Zr and Hf) encapsulation in pure Ge_n (Fig. 6) clusters in the whole range, but there is a remarkably high value of the gap at n=16. In the previous report [15] it is found that the drops are quite marked at n=5, 6, 9, 14, 15, and 17 in Si_nTM (TM = Ti, Zr and Hf) cluster which is different from the present study. Therefore the trend of variation of HOMO-LUMO gap is different in different host for the same transition metal doping.

As mentioned in earlier section, enhanced stability of 20-electron clusters can be rationalized in terms of electronic shell models developed for metal clusters. For metal clusters whenever a new shell starts becoming occupied for the first time, the adiabatic ionization potential (IP) drops sharply [28]. For example, in the report, de Heer [47] has shown that n=20 is a shell field configuration for Li_n clusters and there is a sharp drop in ionization potential when the cluster change from Li_{20} to Li_{21} cluster by absorbing a Li atom in it. If the enhanced stability of the 20-electron $Ge_{16}TM$ cluster is due to a shell field configuration then there should be a sharp drop in IP as one more germanium atom is added to it. This is in particular what we see in the IP variation of Ge_nTi cluster when plotted against n as shown in Fig. 7a. There is a peak in IP at n=16 and then there is a sharp drop from n=16 to 17 and further upto n=20 (not shown). Sharp drop in IP from n=16 to n=17 is perhaps the strongest indication that assumption of a nearly free-electron gas inside the Ge cage is a good model for Ge_nTi clusters, similar to Si_nTM clusters [28]. Variation of IP of the other transition metal clusters is shown in Fig. 7b.

It is well known that chemical stability of the clusters also can be indicated by their electron affinity, which is defined as,

$$EA(eV) = E_{Ge_nTi^-} - E_{Ge_nTi} \tag{7}$$

and is a negative quantity. The clusters those are chemically stable in nature should show relatively low electron affinity. Variation of electron affinity of the Ge_nTi clusters is shown in Fig. 7. It clearly indicating that the electron affinity of the cluster is decreasing for n from n=14 and show a minimum value at n=16 which is a 20 electron cluster. Then there is a sharp increase (in negative sense) of electron affinity from n=16 to 20. Relative dip in EA at n=16 is an indication of enhanced stability of $Ge_{16}Ti$ clusters. Variation of EA of the other transition metal clusters is shown in Fig. 7c.

Further, to verify the chemical stability of Ge_nTi clusters, chemical potential (μ) and chemical hardness (η) of the ground state isomers are calculated. In practice chemical potential and chemical hardness can be expressed in terms of electron affinity and ionization potential. In terms of total energy consideration if E(N) is the energy of the N electron system, then energy of the system containing N+ΔN electrons where ΔN < <N can be expressed as:

$$E(N+\Delta N) = E(N) + \left.\frac{dE}{dx}\right|_{x=N}\Delta N + \frac{1}{2}\left.\frac{d^2E}{dx^2}\right|_{x=N}(\Delta N)^2 + \textit{Neglected higher order terms} \tag{8}$$

Then, μ and η can be defined as:

$$\mu = \left.\frac{dE}{dx}\right|_{x=N} \quad \text{and} \quad \mu = \left.\frac{dE}{dx}\right|_{x=N} \tag{9}$$

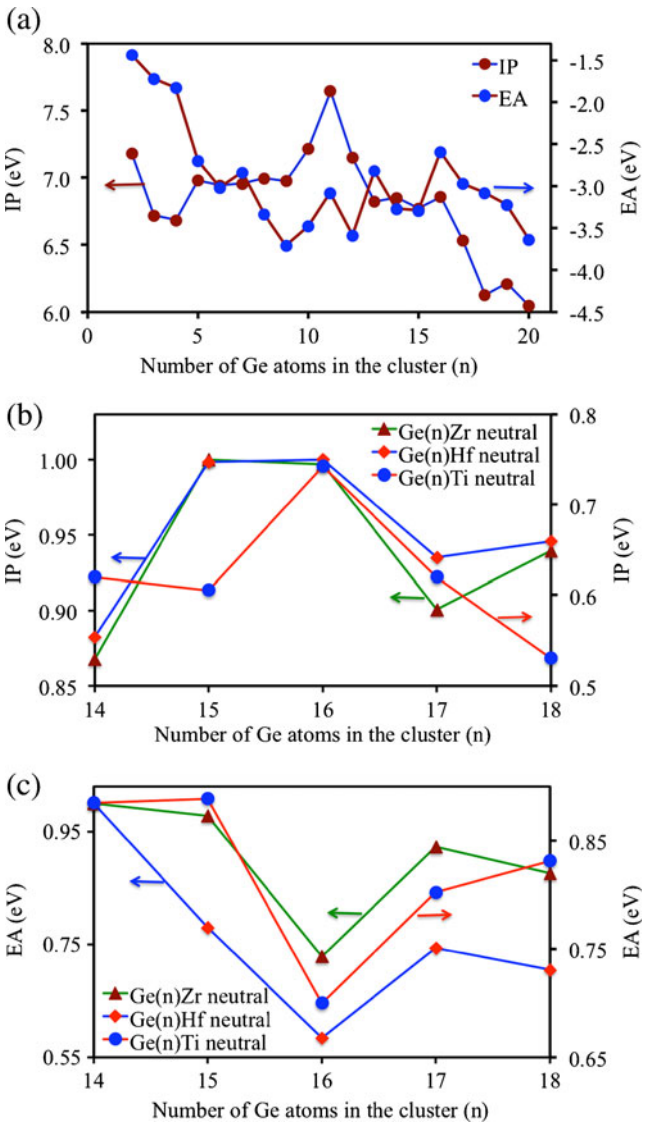

Fig. 7 Variation of IP and EA of Ge_nTi with the size of the cluster (n). All data presented in (**b**) and (**c**) are the normalized values of IP and EA in positive scale respectively

Since, $IP = E(N-1) - E(N)$ and $EA = E(N) - E(N+1)$. By setting $\Delta N = 1$, μ and η are related to IP and EA via the following relations:

$$\mu = -\frac{IP + EA}{2} \text{ and } \eta = \frac{IP - EA}{2} \tag{10}$$

Consider two systems with μ_i and η_i (i=1,2) contracting each other, where some amount of electronic charge (ΔQ) transfer from one to other. The quantity ΔQ and the resultant energy change (ΔE) due to the charge transfer can be determined in the following way:

If E (N+ΔQ) is the energy of the system after charge transfer then it can be expressed for the two different systems 1 and 2 in the following way:

$$E_1(N_1 + \Delta Q) = E_1(N_1) + \mu_1(\Delta Q) + \eta_1(\Delta Q)^2 \tag{11}$$

and

$$E_2(N_2 - \Delta Q) = E_2(N_2) - \mu_2(\Delta Q) + \eta_2(\Delta Q)^2 \tag{12}$$

Corresponding chemical potential becomes, $\mu_1' = \frac{dE_1(x+\Delta Q)}{dx}\Big|_{x=N_1} = \mu_1 + 2\eta_1\Delta Q$ and $\mu_2' = \frac{dE_2(x-\Delta Q)}{dx}\Big|_{x=N_2} = \mu_2 - 2\eta_2\Delta Q$ to first order in ΔM after the charge transfer. In chemical equilibrium, $\mu_1' = \mu_2'$ which gives the following expressions:

$$\Delta Q = \frac{\mu_2 - \mu_1}{2(\eta_1 + \eta_2)} \quad \text{and} \quad \Delta E = \frac{(\mu_2 - \mu_1)^2}{2(\eta_1 + \eta_2)} \tag{13}$$

In the expression, ΔE is the energy gain by the total system (1 and 2) due to exclusive alignment of chemical potential of the two systems at the same value. From the above expression of ΔQ and ΔE it is clear that for easier charge transfer from one system to another it is necessary to have a large difference in μ together with low η_1 and η_2. Therefore, ΔQ and ΔE can be taken as the measure factors to get the idea about the reaction affinity between two systems. Since they are function of the chemical potential and chemical hardness related to the system, so it is important to calculate these parameters of a system to know about its chemical stabilities in a particular environment.

Keeping the above preliminaries in mind, chemical potential (μ) and chemical hardness (η) for Ti doped Ge_n clusters is calculated. To search for the chemical stability of a cluster in chemical reaction or ability to accept electron with low chemical hardness, the |μ/η| ratio along with the chemical potential and chemical hardness is calculated (both of these parameters is normalized to 1) and presented in Fig. 8 with the variation of the size of the cluster. In the Fig. 8 these three parameters are plotted in positive sense. Peak at n=16 in normalized chemical potential plot is actually indicating low value of chemical potential and hence low affinity of the system to take part in chemical reaction in a particular environment. Again at n=16, the presence of a localized dip in normalized chemical hardness plot is also supporting the result of low chemical affection $Ti@Ge_{16}$ cluster. The ratio of these two parameters in positive sense shows a peak and hence indicating the low chemical affinity. Since n=16 is a 20-electron cluster, it is clear that this cluster also show very low affinity in chemical reaction and is in stability agreement with the other parameters.

To get the idea about the vibrational and optical properties of the $TM@Ge_n$ clusters, vibrational (IR) and Raman spectra of optimized ground state isomers are calculated. Some selected ground state clusters for n=15, 16, and 17 are presented in Fig. 9. In the figure the cluster geometry and corresponding most dominating frequencies of IR and Raman spectra are also presented. The absence of any imaginary frequency in the spectrum represents the real nature of the clusters. Careful observation shows the presence of two types of frequencies in IR and Raman spectra of the clusters. The dominant peaks shown in the IR spectra of different clusters are due to the vibration of the germanium atoms in the cage with the transition metal atom as a coupled oscillation, whereas dominant peak in Raman spectrum is only due to the vibration of germanium atoms in the cage. This mode is known as breathing mode in the Raman spectrum where all germanium atoms vibrate in phase. Comparing this with the binding energy graph, it can be seen that the increase in average bond energies (not presented) helps to increase the binding energy per atom in the clusters. It is observed that for both IR and Raman spectra for n=15 and 16 are very clear and a number of modes present also much smaller than $TM@Ge_{17}$ clusters. This is because of the symmetrical nature of n=15 and 16 clusters. It is observed that in a particular size the dominating frequency of IR spectrum decreases from Ti to Hf. It is also observed that the frequency of the

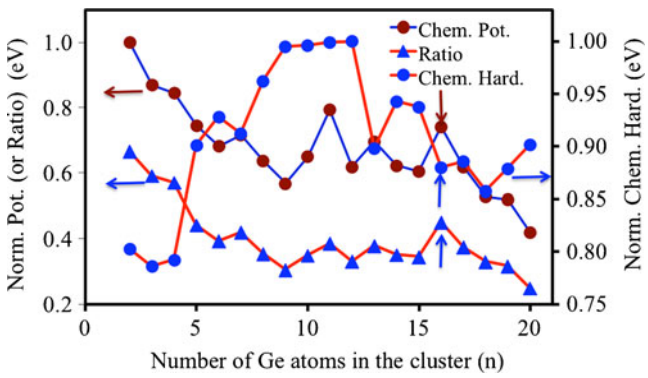

Fig. 8 Variation of chemical potential, chemical hardness and their ratio of Ge_nTi with the size of the cluster (n). In the figure vertical arrows represent the position of 20-electron clusters

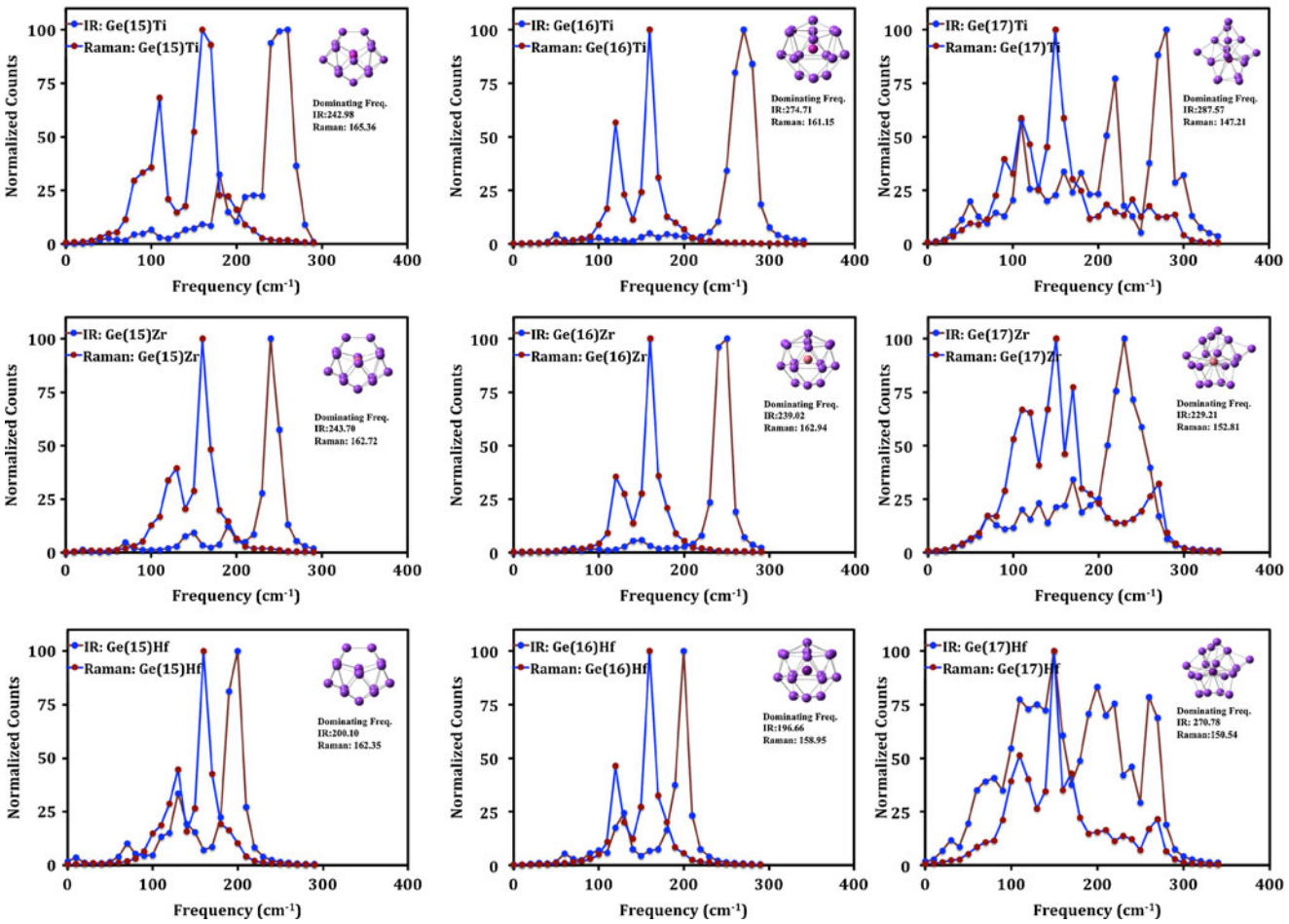

Fig. 9 IR and Raman spectrum of some selected TM@Ge_n clusters

dominating mode in IR spectrum is always much higher than the dominating mode present in Raman spectrum of a particular cluster within the size range n=15 to 17. In a particular size maximum variation of the frequency of the dominating mode in Raman spectrum is 147 cm^{-1} to 166 cm^{-1}, but this range is comparatively much higher in IR spectrum.

Conclusions

In summary, the study of electronic structures and stabilities of transition metal doped germanium nanoclusters is presented. Different properties of neutral and anionic TM-doped optimized geometries of the clusters, like binding energies, stabilities, HOMO-LUMO gap, electron affinities, ionization potentials, charge transfer, infrared and Raman spectra are discussed. Based on the results, the following conclusions can be made:

a) It is always favorable to attach a TM-atom to Ge clusters at all sizes, as the EE turns out to be negative (as according to the definition of the EE in the present study) in every case of neutral and anionic clusters. All clusters with size n>9 absorb TM atom endohedrally in the cage of Ge_n pure cluster. In all TM-doped clusters beyond $n>7$, the spin on the TM atom is quenched.

b) More interesting is the relative stability of these clusters. As measured by their BE, EE, Δ(n,n-1) and $\Delta_2(n)$, both neutral and anionic clusters having 20 valence electrons show enhanced stability, in agreement with shell model predictions. It also shows up in the IP values of the Ge_nTi clusters, as there is a sharp drop in IP from n=16 to 17. Validity of nearly free-electron shell model is similar to that of transition metal doped silicon clusters. While $Ge_{16}Ti$ is particularly a stable species, $Ge_{15}Ti$ with its smaller IP may form ionic compounds with halogen atoms. Although the signature of stability is not so sharp in the HOMO-LUMO gaps of the anionic cluster, but there is still a local maximum at n=15, indicating enhanced stability of a 20-electron cluster, but this signature is very prominent for n=16 in neutral cluster which is also a 20-electron cluster. Other parameters like, EA, chemical

potential are related to the chemical stabilities of the neutral cluster for n=16 also supports the identical stability nature of the clusters. Identification of such stable species, and variation of chemical properties with size in the transition metal doped germanium clusters will help to design germanium-based superatoms. The present work is the preliminary step in the direction of designing of transition metal doped germanium superatoms and it will be followed by more detailed studies on different other systems with bigger cluster sizes.

c) Infrared intensities and Raman activities show distinct spectra for different optimized clusters. This also reflects the change of bonding nature with the size of the clusters. This can be useful to identify the structures of these clusters from experiments. IR and Raman spectra do not show any imaginary frequency in optimized ground state. Moreover, it shows that the number of modes present in the IR and Raman spectrum in symmetric clusters is less compared to the less symmetric clusters. Since there are different dominating frequencies present in IR range of the vibrational spectrum of the cluster which is a function of the size and the nature of transition metal doping, therefore this data is very much important to design a transition metal doped hybrid germanium IR sensitive nano device or helpful to design other types of germanium-transition metal based nano devices.

Acknowledgments Complete computations using Gaussian 03 were performed at the cluster computing facility, Harish-Chandra Research Institute, Allahabad, UP, India (http://cluster.hri.res.in).

References

1. Ho KM, Shvartsberg AA, Pan B, Lu ZY, Wang CZ, Wacker JG, Fye JL, Jarrod MF (1998) Nature 392:582–585
2. Wang J, Chen X, Liu JH (2008) J Phys Chem A 112:8868–8876
3. Zhao WJ, Wang YX (2008) Chem Phys 352:291–296
4. Jarrold MF, Constant VA (1991) Phys Rev Lett 67:2994–2997
5. Benedict LX, Puzer A, Willimson AJ, Grossman JC, Galli G, Klepeis JE, Raty JY, Pankratov O (2003) Phys Rev B 68:85310–85317
6. Brown WL, Freeman RR, Raghavachari K, Schluter M (1987) Science 235:860–865
7. Hiura H, Miyazaki T, Kanayama T (2001) Phys Rev Lett 86:1733–1736
8. Hayashi S, Kanzaya Y, Kataoka M, Nagarede T, Yamamoto K (1993) Z Phys D Atom Mol Cl 26:144–146
9. Bandyopadhyay D, Kaur P, Sen P (2010) J Phys Chem A 114:12986–12991
10. Polman A (2002) Nat Matters 1:10–12
11. Bandyopadhyay D, Sen P (2010) J Phys Chem A 114:1835–1842
12. Jarrold MF, Bower JE (1992) J Chem Phys 96:9180–9190
13. Kumar V, Kawazoe Y (2001) Phys Rev Lett 87:045503–045506
14. Kumar V, Kawazoe Y (2002) Phys Rev Lett 88:235504–235507
15. Bandyopadhyay D (2008) J Appl Phys 104:084308–084314
16. Bandyopadhyay D (2009) Mol Simul 35:381–394
17. Kumar M, Bandyopadhyay D (2008) Chem Phys 353:170–176
18. Beck SM (1987) J Chem Phys 87:4233–4234
19. Beck SM (1989) J Chem Phys 90:6306–6312
20. Ohara M, Miyajima K, Pramann A, Nakajima A, Kaya K (2002) J Phys Chem A 106:3702–3705
21. Han JG (2000) Chem Phys Lett 324:143–148
22. Wang JL, Wang GH, Zhao JJ (2001) Phys Rev B 64:205411–305415
23. Hou XJ, Gopakumar G, Lievens P, Nguyen MT (2997) J Phys Chem A 111:13544–13553
24. Negishi Y, Kawamata H, Hayase T, Gomei T, Kishi R, Hayakawa F, Nakajima A, Kaya K (1997) Chem Phys Lett 269:199–207
25. Bandyopadhyay D (2009) Nanotechnology 20:275202–275213
26. Huheey JE, Keiter EA, Keiter RL (2000) Inorganic Chemistry: principles of structure and reactivity, 4th edn. Harper-Collins College Publisher, New York
27. Sen P, Mitas L (2003) Phys Rev B 68:155404–155407
28. Reveles JU, Khanna SN (2005) Phys Rev B 72:165413–165418
29. Guo LJ, Zhao G, Gu Y, Liu X, Zeng Z (2008) Phys Rev B 77:195417–195424
30. Wigner E, Witmer EE (1928) Z Phys 51:859–886
31. Koyasu K, Akutsu M, Mitsui M, Nakajima A (2005) J Am Chem Soc 127:4998–4999
32. Kumar V (2003) Eur Phys J D 24:227–232
33. Burke K, Perdew JP et al. (1998) In: Dobson JF, Vignale G, Das MP (eds) Electronic Density Functional Theory: Recent Progress and New Directions. Plenum
34. Perdew JP (1991) In: Ziesche P, Eschrig H (eds) Electronic Structure of solids '91. Akademie, Berlin
35. Becke AD (1988) Phys Rev A 38:3098–3100
36. Lee C, Yang W, Parr RG (1988) Phys Rev B 37:785–789
37. Wang J, Han GJ (2005) J Chem Phys 123:064306–064321
38. Han JG, Hagelberg F (2001) J Mol Struct THEOCHEM 549:165–180
39. Guo P, Ren ZY, Wang F, Bian J, Han JG, Wang GH (2004) J Chem Phys 121:12265–12275
40. Guo LJ, Liu X, Zhaoa GF, Luo YH (2007) J Chem Phys 126:234704–234710
41. Nagendran S, Sen SS, Roesky HW, Koley D, Grubmüller H, Pal A, Herbst-Irmer R (2008) Organometallics 27:5459–5463
42. Khon W, Sham LJ (1965) Phys Rev 140:A1133–A1138
43. Kudin KN, Strain MC, Farkas O, Tomasi J, Barone V, Cossi M, Cammi R, Mennucci B, Pomelli C, Adamo C, Clifford S, Ochterski J, Petersson GA, Ayala PY, Cui Q, Morokuma K, Malick DK, Rabuck AD, Raghavachari K, Foresman JB, Cioslowski J, Ortiz JV, Baboul AG, Stefanov BB, Liu B, Liashenko A, Piskorz P, Komaromi I, Gomperts R, Martin RL, Fox DJ, Keith T, Al-Laham MA, Peng CY, Nanayakkara A, Challacombe M, Gill PMW, Johnson B, Chen W, Wong MW, Andres JL, Gonzalez C, Head-Gordon M, Replogle ES, Pople JA (2004) Gaussian 03, Revision E.01. Gaussian, Inc, Wallingford, CT
44. Lu J, Nagase S (2003) Chem Phys Lett 372:394–398
45. Kumar V, Kawazoe Y (2002) Appl Phys Lett 80:859–861
46. Kumar V, Kawazoe Y (2007) Phys Rev B 75:155425–155435
47. de Heer WA (1993) Rev Mod Phys 65:611–676